PALEOMAGNETIC STABILITY

With the background information gained to this point, you appreciate the importance of isolating the characteristic NRM by selective removal of the secondary NRM. Theory and application of paleomagnetic stability tests are introduced here. Partial demagnetization experiments are performed in the laboratory to isolate the ChRM. Although sometimes mistaken as "magic," these laboratory procedures are well grounded in rock magnetism theory. Field tests of paleomagnetic stability can sometimes provide crucial information about the age of a ChRM, and this question is often at the heart of paleomagnetic investigations. Lack of background in paleomagnetic stability tests often prevents interested earth scientists from understanding paleomagnetism. The material in this chapter should largely remove this obstacle. If not a "Big Enchilada," this chapter certainly qualifies as a "Burro Grande."

PARTIAL DEMAGNETIZATION TECHNIQUES

Theory and application of alternating-field and thermal demagnetization are introduced in this section. Although a central part of paleomagnetic investigations for some time, analysis of partial demagnetization data has become more sophisticated because of widespread availability of microcomputer systems for data analysis. Understanding modern paleomagnetism requires some familiarity with the analytical techniques that are used to decipher potentially complex, multicomponent NRM. To put the theory and techniques into practice, this section concludes with some practical examples.

Theory of alternating-field demagnetization

The fundamental AF demagnetization procedure is to expose a specimen to an alternating magnetic field. The waveform of the alternating magnetic field is a sinusoid with linear decrease in magnitude with time. Maximum value of this AF demagnetizing field can be labeled H_{AF} and the waveform is schematically represented in Figure 5.1a.

Typical instruments allow AF demagnetization to maximum H_{AF} of 1000 Oe (100 mT). The frequency of the sinusoidal waveform is commonly 400 Hz, and the time for decay of the field from maximum value to zero is ~1 minute. Most AF demagnetizing instruments use a *tumbler apparatus* that rotates the sample within several nested gears. The tumbler is designed to present in sequence all axes of the specimen to the axis of the demagnetizing coil. The tumbler thus allows demagnetization of all axes of the specimen during the course of a single demagnetization treatment.

The basic theory of AF demagnetization can be explained with the aid of Figure 5.1b, a blow-up of a portion of the AF demagnetization waveform. Imagine that the magnetic field at point 1 (Figure 5.1b) has magnitude = 200 Oe (20 mT) and that we arbitrarily define this direction as "up." Magnetic moments of all grains in the specimen with $h_c \leq 200$ Oe (20 mT) will be forced to point in the up direction. The magnetic field then passes through zero to a maximum in the opposite direction. If the magnitude of the sinusoidal magnetic field decreases by 1 Oe every half cycle, the field at point 2 will be 199 Oe (19.9 mT) in the "down" direction, and all grains with $h_c \leq 199$ Oe (19.9 mT) will have magnetic moment pulled into the down direc-
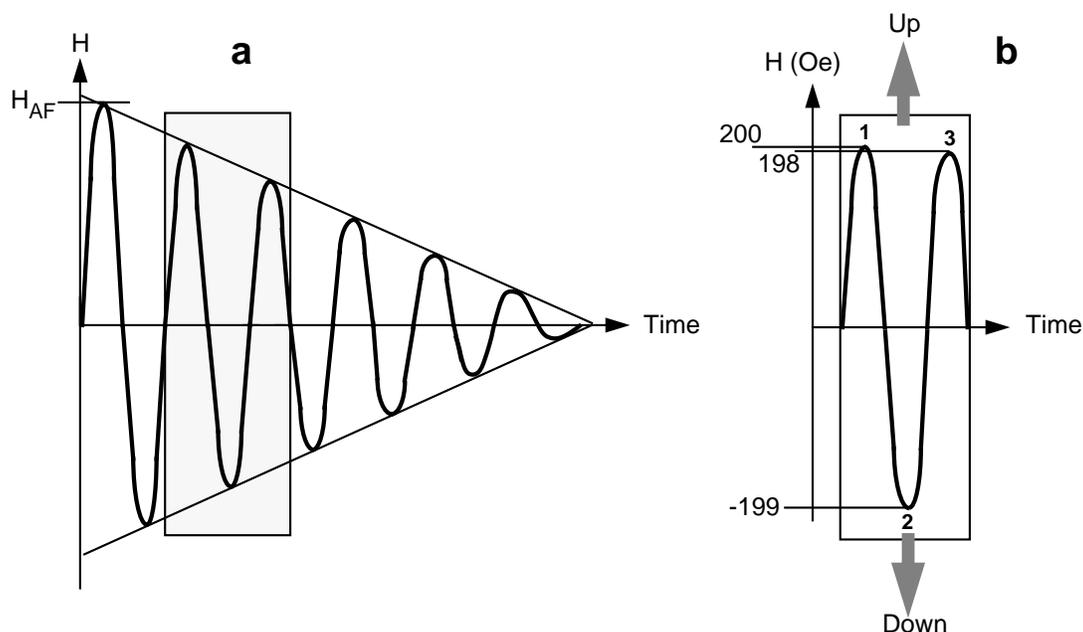
Figure 5.1 Schematic representation of alternating-field demagnetization. (**a**) Generalized waveform of the magnetic field used in alternating-field (AF) demagnetization showing magnetic field versus time; the waveform is a sinusoid with linear decay in amplitude; the maximum amplitude of magnetic field (= peak field) is H_{AF}; the stippled region is amplified in part (**b**). (**b**) Detailed examination of a portion of the AF demagnetization waveform. Two successive peaks and an intervening trough of the magnetic field are shown as a function of time; the peak field at point 1 is 200 Oe; the peak field at point 2 is –199 Oe; the peak field at point 3 is 198 Oe.

tion. After point 2, the magnetic field will pass through zero and increase to 198 Oe (19.8 mT) in the up direction at point 3. Now all grains with $h_c \leq 198$ Oe (19.8 mT) have magnetic moment pointing up.

From point 1 to point 3, the net effect is that grains with h_c in the interval 199 to 200 Oe (19.9 to 20 mT) are left with magnetic moments pointing up, while grains with h_c between 198 and 199 Oe (19.8 to 19.9 mT) are left with magnetic moments pointing down. The total magnetic moments of grains in these two h_c intervals will approximately cancel one another. Thus the net contribution of all grains with $h_c \leq H_{AF}$ will be destroyed; only the NRM carried by grains of $h_c \geq H_{AF}$ will remain. Because the tumbler apparatus presents all axes of the specimen to the demagnetizing field, the NRM contained in all grains with $h_c \leq H_{AF}$ is effectively randomized. Thus, AF demagnetization can be used to erase NRM carried by grains with coercivities less than the peak demagnetizing field.

AF demagnetization is often effective in removing secondary NRM and isolating characteristic NRM (ChRM) in rocks with titanomagnetite as the dominant ferromagnetic mineral. In such rocks, secondary NRM is dominantly carried by MD grains, while ChRM is retained by SD or PSD grains. MD grains have h_c dominantly ≤ 200 Oe (20 mT), while SD and PSD grains have higher h_c. AF demagnetization thus can remove a secondary NRM carried by the low h_c grains and leave the ChRM unaffected. AF demagnetization is a convenient technique because of speed and ease of operation and is thus preferred over other techniques when it can be shown to be effective.

Theory of thermal demagnetization

The procedure for thermal demagnetization involves heating a specimen to an elevated temperature (T_{demag}) below the Curie temperature of the constituent ferromagnetic minerals, then cooling to room temperature in zero magnetic field. This causes all grains with blocking temperature (T_B) $\leq T_{demag}$ to acquire a "thermoremanent magnetization" in $H = 0$, thereby erasing the NRM carried by these grains. In other words, the

magnetization of all grains for which $T_B \leq T_{demag}$ is randomized, as with low h_c grains during AF demagnetization.

The theory of selective removal of secondary NRM (generally VRM) by partial thermal demagnetization is illustrated in the v–h_c diagram of Figure 5.2. As described in discussion of VRM, SD grains with short
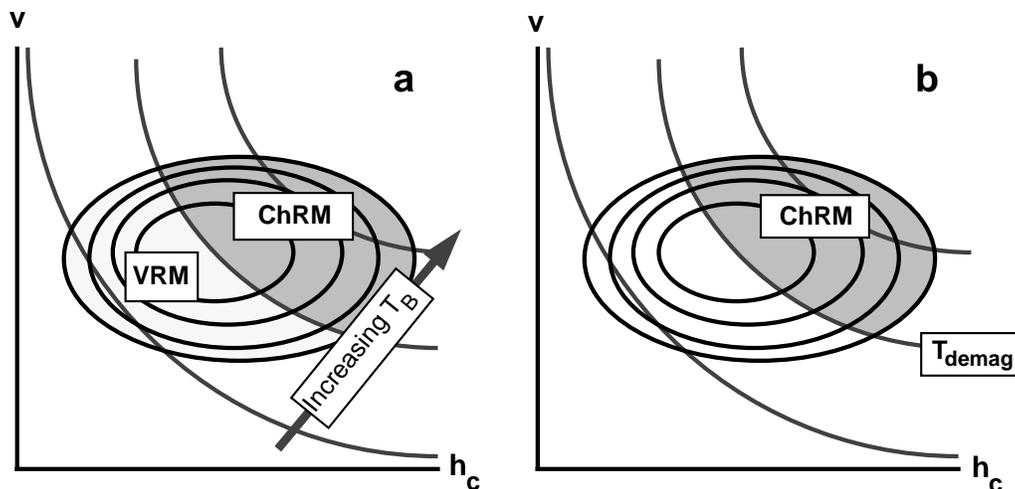
Figure 5.2 Schematic explanation of thermal demagnetization. (**a**) Diagram plots grain volume (v) versus microscopic coercive force (h_c) for a hypothetical population of SD grains. Solid contours are of concentration of SD grains; stippled lines are contours of τ (and T_B) with values increasing from lower left to upper right; grains with low τ and low T_B preferentially carry VRM; these grains occupy the lightly stippled region in the lower left portion of the diagram; grains with high τ and high T_B preferentially carry ChRM; these grains occupy the heavily stippled region. (**b**) Following thermal demagnetization to temperature T_{demag}, NRM in SD grains with $T_B < T_{demag}$ is erased. Only the ChRM in the SD grains with higher T_B remains.

relaxation time, τ, can acquire VRM, while SD grains with long τ are stable against acquisition of VRM. In the development of TVRM in Chapter 3, it was shown that SD grains with short τ also have low T_B and this is the fundamental principle underlying partial thermal demagnetization. Lines of equal τ on a v–h_c diagram are also lines of equal T_B and SD grains which predominantly carry VRM also have low T_B. This situation is schematically represented in Figure 5.2a. The effectiveness of thermal demagnetization in erasing VRM can be understood by realizing that thermal demagnetization to $T_{demag} \geq T_B$ of grains carrying VRM will selectively erase VRM, leaving unaffected the ChRM carried by grains with longer τ (= higher T_B).

The above descriptions of AF and thermal demagnetization explain why AF demagnetization generally fails to remove secondary NRM components from hematite-bearing rocks. The property common to grains carrying secondary NRM in hematite-bearing rocks is low τ resulting from low <u>product</u> $v \cdot h_c$. Grains with high h_c but small volume, v, can carry secondary NRM. But these grains would not be erased by AF demagnetization because their coercive force could easily exceed the maximum available field H_{AF}. Therefore, in rocks with hematite as the dominant ferromagnetic mineral, removal of VRM invariably requires thermal demagnetization.

Chemical demagnetization

Leaching of rocks with dilute acids (usually hydrochloric) gradually dissolves FeTi-oxides. Acid leaching of rock specimens for progressively increasing time intervals is called *chemical demagnetization*. Because of high surface area to volume ratio for small grains, chemical demagnetization preferentially removes the small grains. The technique is effective in removing hematite pigment and microcrystalline hematite in red

sediments. This selective removal of fine-grained hematite means that chemical demagnetization can remove secondary NRM commonly carried by these grains in red sediments. Chemical demagnetization and thermal demagnetization usually accomplish the same removal of secondary NRM, leaving the ChRM. Because chemical demagnetization is an inherently messy and time-consuming process, thermal demagnetization is the preferred technique.

Progressive demagnetization techniques

In this section, we deal with the following questions:

1. How does one determine the best demagnetization technique to isolate the ChRM in a particular suite of samples?
2. What is the appropriate demagnetization level (H_{AF} or T_{demag}) for isolating the ChRM?

Progressive demagnetization experiments are intended to provide answers to these all-important questions. These experiments are usually performed following measurement of NRM of all specimens in a collection. Distributions of NRM directions provide information about likely secondary components, while knowledge of ferromagnetic mineralogy can indicate which demagnetization technique is likely to provide isolation of components of NRM.

The general procedure in progressive demagnetization is to sequentially demagnetize a specimen at progressively higher levels, measuring remaining NRM following each demagnetization. A generally adopted procedure is to apply progressive AF demagnetization to some specimens and progressive thermal demagnetization to other specimens. This procedure allows comparison of results obtained by the two techniques. The objective is to reveal *components* of NRM that are carried by ferromagnetic grains within a particular interval of coercivity or blocking temperature. Resistance to demagnetization is often discussed in terms of *stability* of NRM, with *low-stability components* easily demagnetized and *high-stability components* removed only at high levels of demagnetization.

Adequate description of components of NRM usually requires progressive demagnetization at a minimum of eight to ten levels. Exact levels of demagnetization are usually adjusted in a trial-and-error fashion. However, a general observation is that coercivities are log-normally distributed so that initially small increments in peak field of AF demagnetization are followed by larger increases at higher levels. A typical progression would be peak fields of 10, 25, 50, 100, 150, 200, 300, 400, 600, 800, and 1000 Oe.

In progressive thermal demagnetization, temperature steps are distributed between ambient temperature and the highest Curie temperature. A typical strategy is to use temperatures increasing in 50°C to 100°C steps at low temperatures but smaller temperature increments (sometimes as small as 5°C) within about 100°C of the Curie temperature. The end product of a progressive demagnetization experiment is a set of measurements of NRM remaining after increasing demagnetization levels. Analysis of these data require procedures for displaying the progressive changes in both direction and magnitude of NRM.

Graphical displays

To introduce various techniques of graphical display, consider the example of progressive demagnetization results shown in the idealized perspective diagram of Figure 5.3. Although highly simplified, this example was abstracted from actual observations and does display the fundamental observations that are typical of a common two-component NRM. Each NRM vector is labeled with a number corresponding to the demagnetization level with point 0 indicating NRM prior to demagnetization. During demagnetization at levels 1 through 3, the remaining NRM rotates in direction and changes intensity as a low-stability component is removed. This low-stability component of NRM is depicted by the dashed arrow in Figure 5.3 and can be determined by the vector subtraction

$$NRM_{0-3} = NRM_0 - NRM_3 \qquad (5.1)$$
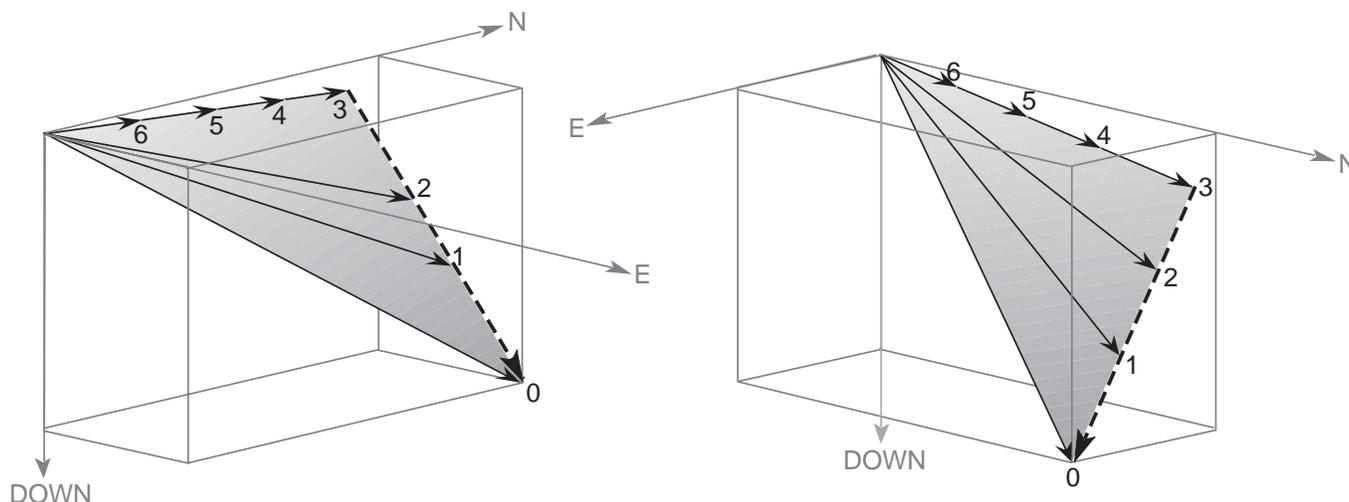
Figure 5.3 Perspective diagram of NRM vector during progressive demagnetization. Geographic axes are shown; solid arrows show the NRM vector during demagnetization at levels 0 through 6; the dashed arrow is the low-stability NRM component removed during demagnetization at levels 1 through 3; during demagnetization at levels 4 through 6, the high-stability NRM component decreases in intensity but does not change in direction.

where **NRM$_0$** and **NRM$_3$** are NRM at demagnetization levels 0 and 3.

During demagnetization at levels 4 through 6, remaining **NRM** does not change in direction but decreases in intensity. This high-stability component is successfully isolated by demagnetization to level 3 and, if observed for a number of specimens, would be taken as the ChRM. Notice that the end of the NRM vector describes a line toward the origin during demagnetization at levels 4 through 6. Observing a linear trajectory of the vector end point toward the origin is a key to recognizing that a high-stability NRM component has been isolated.

Graphical techniques that allow changes in three-dimensional vectors to be displayed on a two-dimensional page are required for analysis of progressive demagnetization results. All such graphical techniques require some sort of projection, and all have attributes and limitations.

The progressive demagnetization information of Figure 5.3 is shown in Figure 5.4, using the technique generally applied until the mid-1970s. An equal-area projection is used to display the direction of the NRM vector (Figure 5.4a), while changes in intensity of NRM are plotted separately (Figure 5.4b). The direction of NRM changes between levels 0 and 3 and is constant during subsequent demagnetization at levels 3 through 6. However, the separation of direction and intensity information makes visualization of the separate NRM components difficult.

Results of progressive demagnetization experiments are now displayed by using one of several forms of a *vector component* (*vector end point* or *orthogonal projection*) *diagram*. The technique was developed by Zijderveld (see Suggested Readings), and the diagram is also referred to as a *Zijderveld diagram*. The power of the vector component diagram is its ability to display directional and intensity information on a single diagram by projecting the vector onto two orthogonal planes. However, an initial investment of time and concentration is required to understand these diagrams. Almost all research articles on paleomagnetism that have been published within the past decade contain at least one vector component diagram. So understanding modern paleomagnetism requires understanding the fundamentals of this graphical technique. We're going to pause now while you go prepare a large pot of black coffee (OK, Britons may use tea). When you've got yourself suitably prepared, dive into the following explanation of vector component diagrams.
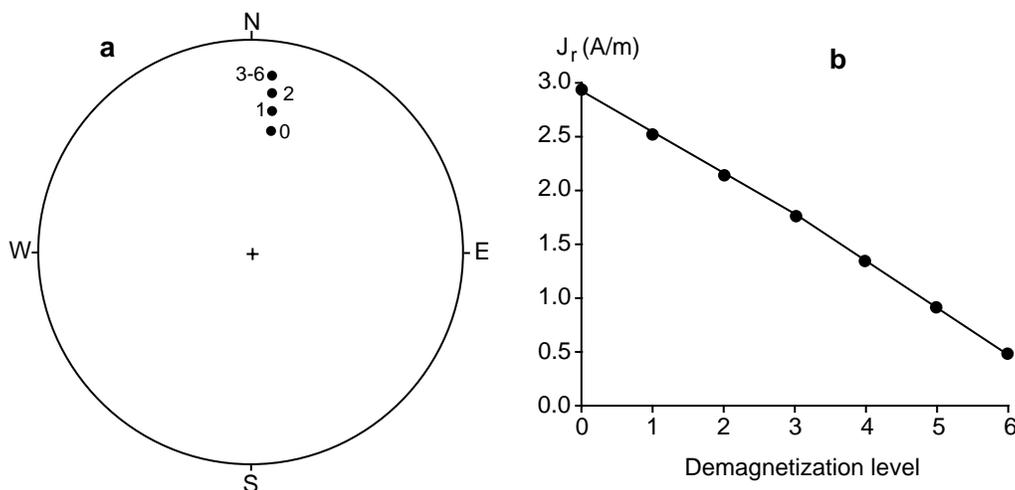
Figure 5.4 Equal-area projection and NRM intensity plot of progressive demagnetization results. (**a**) Equal-area projection of the direction of NRM. Numbers adjacent to NRM directions indicate the demagnetization level; the NRM direction changes between levels 0 and 3 but is constant direction between levels 3 and 6. (**b**) NRM intensity versus demagnetization level. A slight break in slope occurs at demagnetization level 3.

In the vector component diagram, the base of the NRM vector is placed at the origin of a Cartesian coordinate system, and the tip of the vector is projected onto two orthogonal planes. The distance of each data point from the origin is proportional to the intensity of the NRM vector projected onto that plane. To construct a vector component diagram, each NRM vector observed during the progressive demagnetization experiment is decomposed into its north (N), east (E), and vertical (Down) components:

$$N_i = \text{NRM}_i \ \cos I_i \ \cos D_i \tag{5.2}$$

$$E_i = \text{NRM}_i \ \cos I_i \ \sin D_i \tag{5.3}$$

$$Z_i = \text{NRM}_i \ \sin I_i \tag{5.4}$$

where NRM_i is the intensity of **NRM**$_i$, and I_i and D_i are the inclination and declination of **NRM**$_i$.

Figure 5.5 shows the construction of a vector component diagram displaying the progressive demagnetization data of Figure 5.3. In Figure 5.5a, the projection of the seven NRM vectors onto the horizontal plane is constructed by plotting N_i versus E_i; each data point represents the end of the NRM vector projected onto the horizontal plane (hence the name vector end point diagram). As an example, the horizontal projection of NRM_3 is shown by the heavily stippled arrow. The angle between the north axis and a line from the origin to each data point is the declination of the NRM vector at that demagnetization level.

If you examine Figure 5.5a carefully, you observe that points 0 through 3 are collinear and the trajectory of those data points does not intersect the origin. Points 3 through 6 are also collinear, but the trajectory of these points <u>does</u> project toward the origin. These two lines on the horizontal projection of Figure 5.5a are the first indications that the progressive demagnetization data being displayed are the result of two separate components of NRM, one removed between levels 0 to 3 (= NRM_{0-3}) and one removed between levels 3 to 6. In fact, the lightly stippled arrow of Figure 5.5a is the horizontal projection of NRM_{0-3}, while the heavily stippled arrow is the horizontal projection of the ChRM isolated by demagnetization to level 3.

The second projection required to describe the progressive NRM data is on a vertical plane. In Figure 5.5b, the vertical component of the NRM vector at each demagnetization level is plotted against the north component. The actual vertical projection of NRM_0 is shown by the black arrow, while the vertical projection of NRM_3 is shown by the heavily stippled arrow. Figure 5.5b is a view looking directly westward normal to the north-south oriented vertical plane. The vertical component can be shown projected onto a vertical
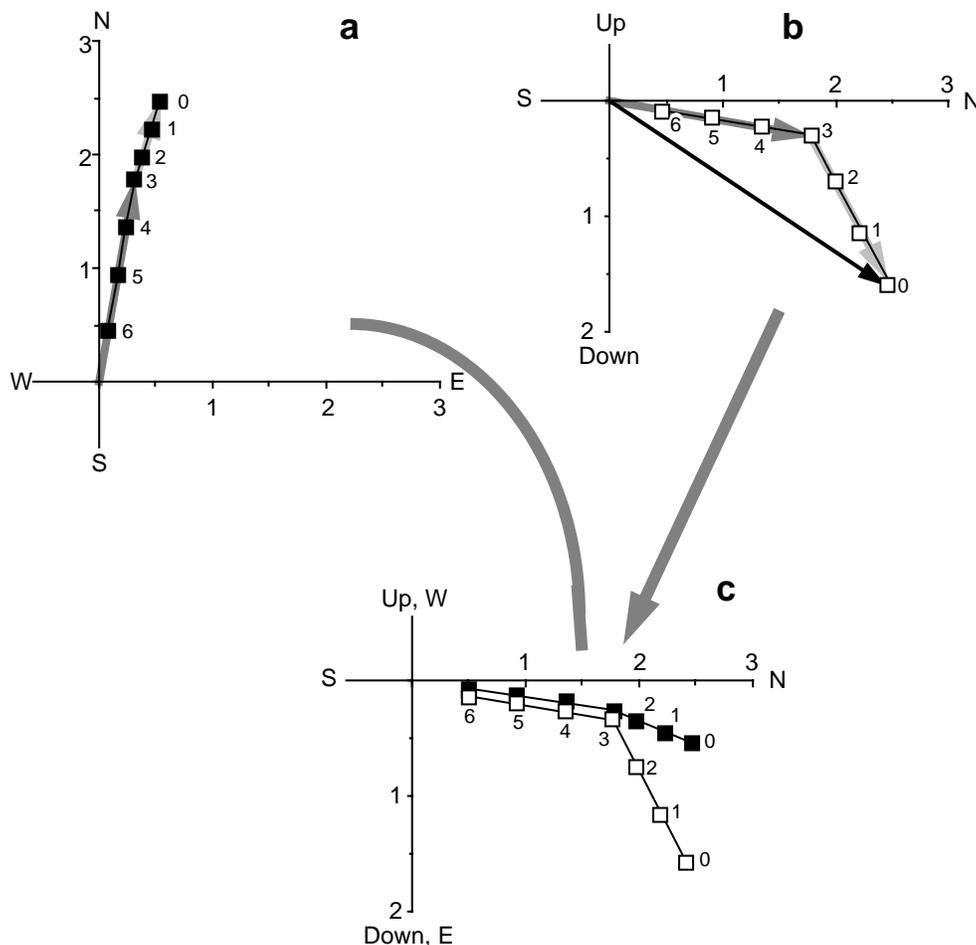
Figure 5.5 Construction of vector component diagram. (**a**) Projection of the NRM vector shown in Figure 5.3 onto the horizontal plane. The scale on the axes is in A/m; the lightly stippled arrow is the horizontal projection of the NRM vector removed during demagnetization at levels 1 through 3; the heavily stippled arrow is the projection of the NRM vector remaining at level 3. (**b**) Projection of the NRM vector onto a vertical plane oriented north-south. The solid arrow is the vertical projection of the NRM vector prior to demagnetization; the lightly stippled arrow is the projection of the NRM vector removed during demagnetization at levels 1 through 3; the heavily stippled arrow is the projection of the NRM vector remaining at level 3. (**c**) Horizontal and vertical projections combined into a single vector component diagram. Solid data points indicate vector end points projected onto the horizontal plane; open data points indicate vector end points projected onto the vertical plane; numbers adjacent to data points are demagnetization levels.

plane oriented north-south (as in this case) or oriented east-west. The choice of the north-south vertical plane (and north axis as abscissa) for Figure 5.5b is made because this vertical plane is closest to the vector being projected.

In Figure 5.5b, the separation of the two components of NRM is clearly displayed by the break in slope of the *end point trajectory* at level 3. Points 0 to 3 are collinear, but the line connecting these points does not include the origin. The vertical projection of the low-stability component removed in this interval is shown by the lightly stippled arrow in Figure 5.5b. Points 3 to 6 also are collinear, and the trajectory of these end points does include the origin, indicating removal of a single vector with constant direction. That vector is of course the ChRM with its vertical projection shown by the heavily stippled arrow.

The importance of observing a trajectory of vector end points that trend toward the origin of a vector component diagram cannot be overemphasized. This is the critical observation, indicating that a single

vector with constant direction is being removed (e.g., Figure 5.3, levels 3 to 6). Observation of a linear trend of end points toward the origin indicates successful removal of the low-stability NRM component allowing isolation of the high-stability ChRM.

It is possible to determine the inclination of ChRM by realizing that the angle between the N axis and the line through points 3 to 6 is the *apparent inclination*, I_{app}, which is related to the true inclination, I, by

$$\tan I = \tan I_{app} \, / \cos D| \tag{5.5}$$

where $| \cos D|$ is the absolute value of cos D. The inclination of the low-stability component could be determined similarly; it too is an apparent inclination on Figure 5.5b. The direction of the low-stability component for this example is $I \approx 60°$, $D \approx 18°$.

The last step in construction of the vector component diagram is to combine the two projections into a single diagram as shown in Figure 5.5c, where only end points of the projections onto the horizontal and vertical planes are shown. This diagram contains two sets of coordinate axes, both clearly labeled. Note that the caption indicates that solid data points represent projections of vector end points onto the horizontal plane, while open data points are projections on the vertical plane. This is a common form of the vector component diagram, but many variations exist. No strict conventions for vector component diagrams exist, so you must read figure captions carefully! In vector component diagrams in this book, horizontal projections are always shown with solid data points, and open data points are used for vertical projections.

From the example of Figure 5.5, the ability of the vector component diagram to reveal components of NRM is apparent. However, this technique has limitations that should be appreciated. If a component of NRM perpendicular to one of the projection planes is removed, that component is not apparent <u>on that projection plane</u>. However, the removed component <u>is</u> apparent in the projection onto the orthogonal plane. For example, if an NRM component pointing directly east is removed, the projection on a north-south oriented vertical plane degenerates to a single point. However, removal of this east-directed component is readily apparent on the horizontal projection. The lesson is that <u>both</u> projections must be scrutinized. Forgetting that these diagrams are geometrical constructs of three-dimensional information can lead to serious errors.

In Figure 5.6, an alternative form of the vector component diagram is shown by using the progressive demagnetization information of Figure 5.3. In this diagram, the horizontal projection (Figure 5.6a) is developed as before (Figure 5.5a). North and east axes are also drawn through point 3 in this diagram to illustrate how the declination of the low-stability component (NRM_{0-3}) can be determined from the diagram. In Figure 5.6b, the vertical plane projection is constructed by plotting the vector on the vertical plane in which it lies. This plane may change orientation for each demagnetization step. This form of the vector component diagram has the advantage that the vertical plane shows true inclination, which can be determined graphically as shown in Figure 5.6b. Also the distance of a data point from the origin of the vertical plane projection is proportional to the <u>total</u> intensity of NRM. However, the shifting declination of the vertical plane can be tricky (and sometimes misleading), and this form of vector component diagram is less popular than the form in Figure 5.5.

Some real examples

Actual examples of progressive demagnetization data are now examined, progressing from fairly simple to complex. Some theoretical explanations for complexities and additional techniques for analysis are introduced.

In Figure 5.7, examples of progressive demagnetization results revealing two-component NRMs of various complexity are illustrated by using vector component diagrams. Figure 5.7a illustrates results from a sample of the Moenave Formation, similar to the idealized Figures 5.3 to 5.6. Thermal demagnetization up to 508°C removes a low-stability component of NRM directed toward the north and downward. Prior to demagnetization, the distribution of sample NRM directions from this site (individual bed of red siltstone)
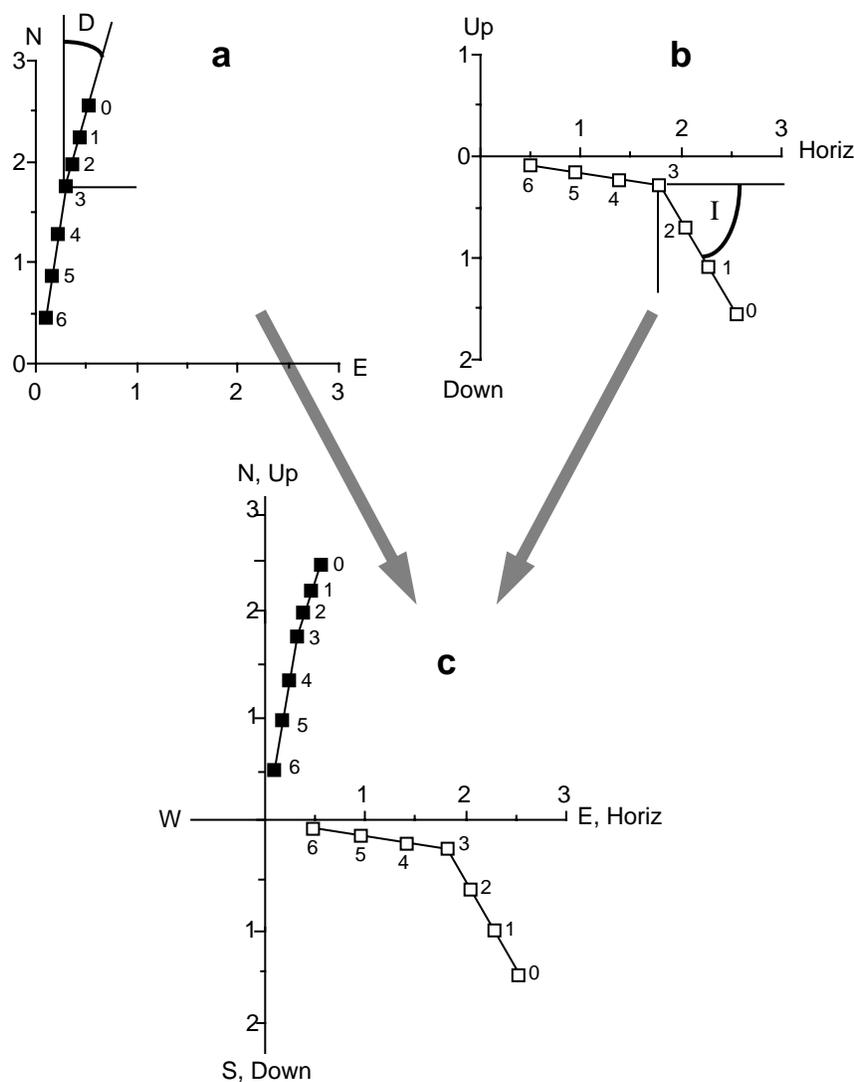
Figure 5.6 Construction of an alternative form of vector component diagram. (**a**) Projection of the NRM
vector shown in Figure 5.3 onto the horizontal plane. This diagram is identical to Figure 5.5a;
angle *D* is the declination of the low-stability NRM component removed during demagnetization at
levels 1 through 3. (**b**) Projection of NRM vector onto a vertical plane cutting directly through the
NRM vector. The scale on the axes is in A/m; the distance of each data point from the origin
indicates the total NRM intensity; angle *I* is the inclination of the low-stability NRM component
removed during demagnetization at levels 1 through 3. (**c**) Horizontal and vertical projections
combined into a single vector component diagram. Solid data points indicate vector end points
projected onto the horizontal plane; open data points indicate vector end points projected onto the
vertical plane; numbers adjacent to data points are demagnetization levels.

shows streaking of directions along a great circle that includes the present geomagnetic field direction at the
sampling locality. The low-stability component thus can be interpreted as a secondary VRM aligned with the
present geomagnetic field.

For demagnetization temperatures from 508° to 690°C, the trajectory of vector end points is along a
linear trend toward the origin. This ChRM points almost directly north with no significant directional change
in the 508° to 690°C interval of demagnetization temperatures. Similar directions were observed during
progressive demagnetization of other samples from this collecting locality. In this case, the two-components
of NRM are sharply separated. The ChRM constitutes a significant portion of total NRM, and there is a
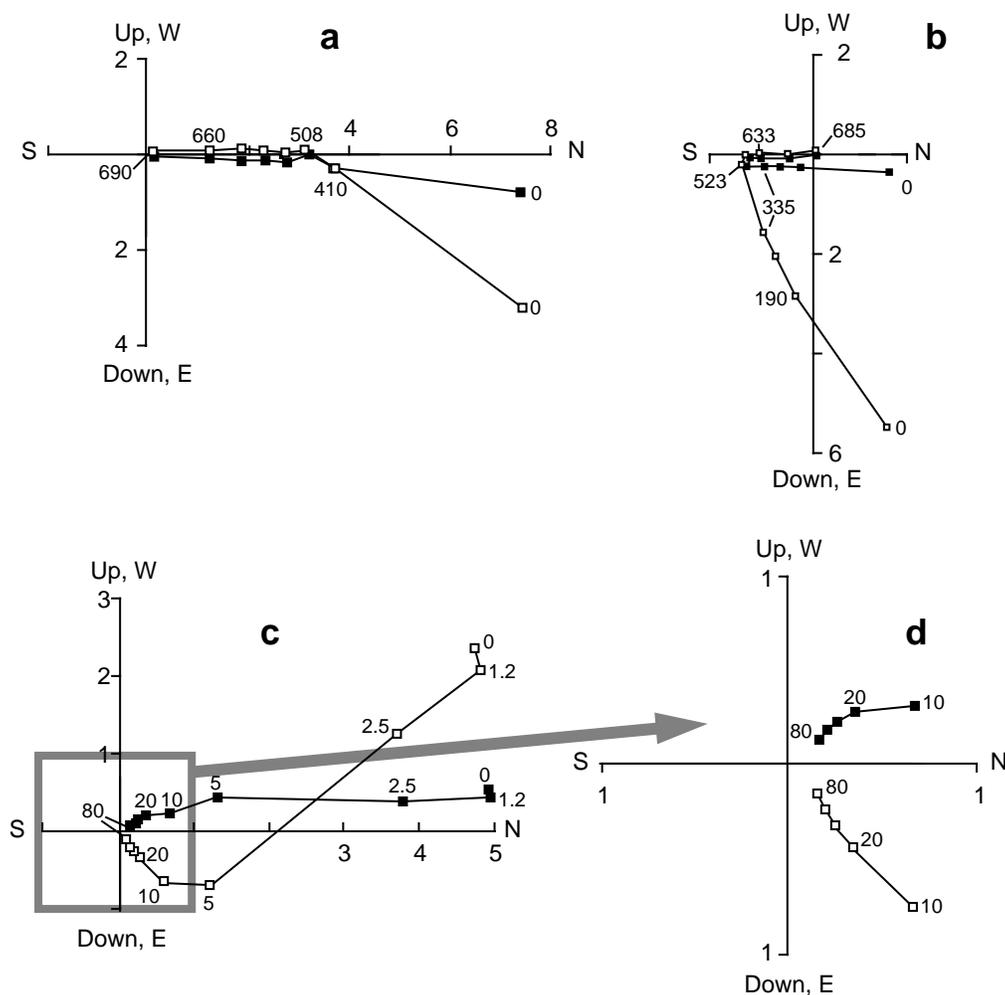
Figure 5.7 Example vector component diagrams. In all diagrams, numbers on axes indicate NRM
intensities in A/m, solid data points indicate projection onto the horizontal plane, and open data
points indicate projection onto the vertical plane. (**a**) Progressive thermal demagnetization of a
sample from the Moenave Formation. Numbers adjacent to data points indicate temperature in
degrees Celsius. (**b**) Progressive thermal demagnetization of a sample from the Chinle Forma-
tion. Numbers adjacent to data points indicate temperature in degrees Celsius.   (**c**) Progressive
AF demagnetization of a sample of Miocene basalt. Numbers adjacent to data points indicate
peak demagnetizing field in mT; region of diagram outlined by stippled box is amplified in part (**d**).

substantial interval of demagnetization temperatures over which the ChRM can be observed. Thermal
demagnetization to any temperature from about 510° to 600°C would effectively remove the low-stability
component, revealing the high-stability ChRM.

In Figures 5.7*c* and 5.7*d*, results of progressive AF demagnetization of a sample of Miocene basalt are
illustrated. Directions of NRM of other samples from this site are highly scattered (similar to Figure 4.7c),
and intensities of NRM are anomalously high. AF demagnetization to a peak field of 20 mT (= 200 Oe)
removes a large low-stability component of NRM directed toward the north with $I \approx -40°$. During AF demag-
netization to peak fields in the 20 to 80 mT interval (200 to 800 Oe; see the enlargement in Figure 5.7d),
vector end points define a trajectory toward the origin with no significant change in direction of remaining
NRM. These observations indicate that ChRM is isolated by AF demagnetization to 20 mT (200 Oe). The
ChRM has a direction: $D \approx 330°$, $I \approx 55°$.

An additional sample from this site was thermally demagnetized following isolation of the ChRM by AF
demagnetization to 20 mT (200 Oe) peak field. Blocking temperatures were dominantly between 450° and

580°C, and the direction of ChRM observed during thermal demagnetization was the same as that observed during AF demagnetization in the 20 to 80 mT interval (200 to 800 Oe). The Curie temperature determined on a sample from this locality was also 580°C, indicating that magnetite is the dominant ferromagnetic mineral. Collectively, these observations indicate that the low-stability NRM component removed by AF demagnetization to 20 mT (200 Oe) is a secondary lightning-induced IRM. The high-stability ChRM isolated during AF demagnetization to peak fields ≥ 20 mT (200 Oe) is a primary TRM acquired during original cooling of this Miocene basalt flow.

A more problematical example is presented in Figure 5.7b. During thermal demagnetization of this Late Triassic red sediment, a large component of NRM is removed during thermal demagnetization to $T \approx 600$°C. This low-stability component ($D \approx 10$°, $I \approx 60$°) is subparallel to the geomagnetic field at the sampling locality and is interpreted as a secondary VRM (or possibly a CRM formed during recent weathering). Only at demagnetization temperatures between 633°C and 685°C is the smaller high-stability ChRM component revealed by the trajectory of vector end points toward the origin. Because the ChRM is smaller than the secondary component of NRM and is isolated only at high demagnetization levels, the ChRM direction cannot be confidently determined from a single specimen. In such cases, determination of the ChRM direction depends critically on internal consistency of results from other samples from the same site.

Overlapping blocking temperature or coercivity spectra

Rather than a sharp corner in the trajectory of vector end points (as in Figure 5.7a), end points often define a curve between the two straight-line segments on the vector component diagram. This complication is due to overlapping blocking temperature spectra (or coercivity spectra) of the ferromagnetic grains carrying the two components of NRM. Curved trajectories can be understood with the aid of Figure 5.8. In this synthetic example, NRM is composed of two components: a low-stability component J_A with direction $D \approx 15$°, $I \approx -25$°; and a high-stability component J_B with direction $D \approx 155$°, $I \approx 70$°. Demagnetization levels (spectra of microscopic coercivity or blocking temperature) over which these components are removed are shown on the left side of Figure 5.8.

In Figure 5.8a, demagnetization spectra of the two components do not overlap; J_A is demagnetized between levels 1 and 6, while J_B is demagnetized between levels 6 and 9. The resulting vector component diagram is shown in Figure 5.8b. Two linear trajectories are observed: one produced by removal of J_A between levels 1 and 6, and another (which includes the origin) produced by removal of J_B between levels 6 and 9. Because the demagnetization spectra of these two components are completely separated, the two trajectories are sharply separated by an acute angle at point 6.

In Figure 5.8c, demagnetization spectra overlap at levels 5 and 6. In the resulting vector component diagram of Figure 5.8d, the two linear trajectories are evident at demagnetization levels 1 to 4 and 7 to 9. However, in the interval of overlap (levels 5 and 6), both components are simultaneously removed, and a curved trajectory develops. The direction of the high-stability J_B component can be determined at demagnetization levels 7 to 9 (i.e., above the overlap).

In Figure 5.8e, demagnetization spectra of the two components are completely overlapping. There is no demagnetization interval over which only one component is removed. The resulting vector component diagram (Figure 5.8f) has no linear segments, and the two components <u>cannot</u> be separated. Although some advanced techniques have been developed in attempts to deal with severely overlapping demagnetization spectra (see below), the situation is usually hopeless, and you might as well drown your sorrows at a local watering hole.

Fortunately, many rocks provide clear separation of components of NRM and confident determination of ChRM. One hopes to observe behaviors like those in Figures 5.7a; often one observes more difficult, but manageable, behaviors such as those in Figures 5.7b, 5.7c, and 5.7d; and one occasionally observes demagnetization behaviors that prevent isolation of a ChRM.
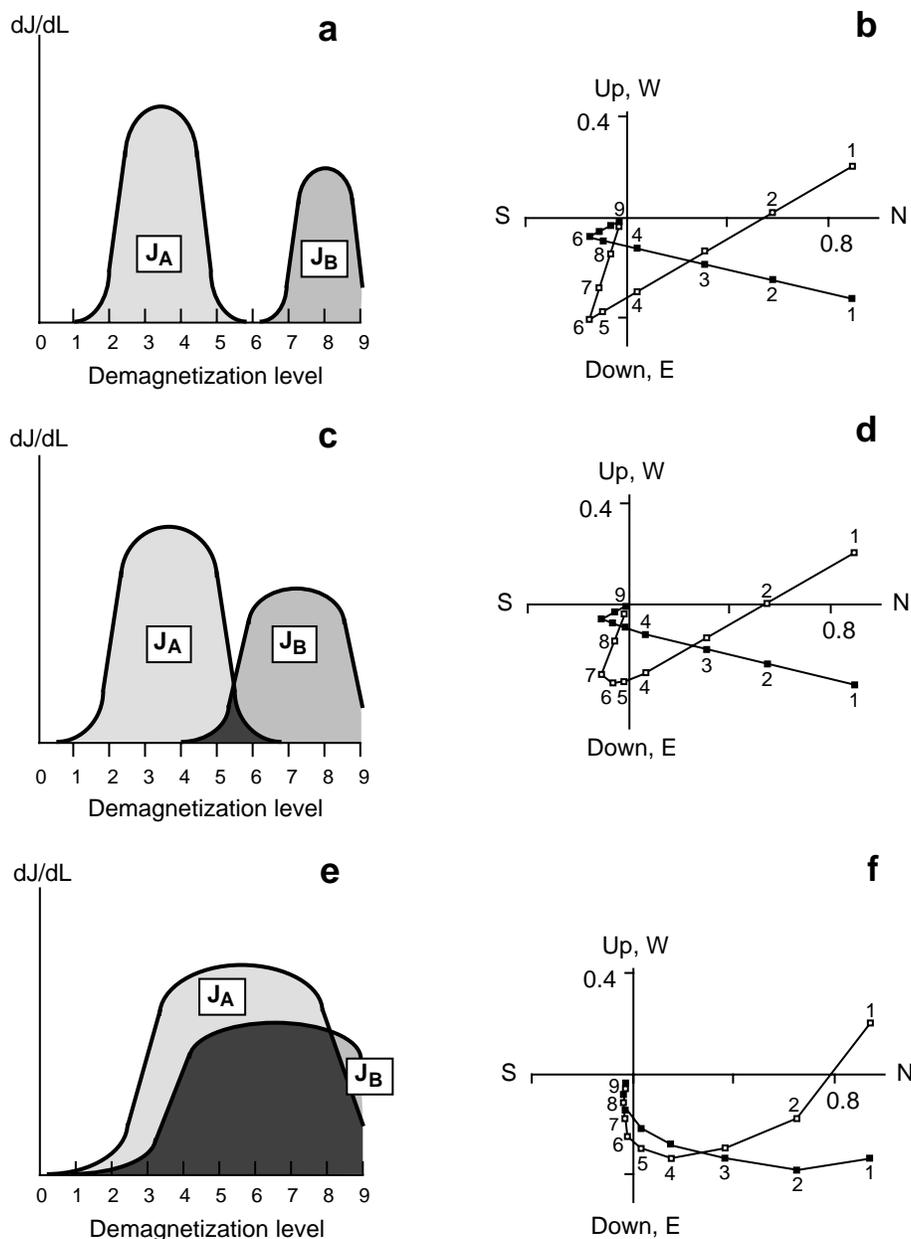
Figure 5.8 Schematic representation of effects of overlapping demagnetization spectra. A lower-stability component, J_A, has direction $I = -25°$, $D = 15°$. A higher-stability component, J_B, has direction $I = 70°$, $D = 155°$. (**a**) Demagnetization spectra of the two NRM components. NRM component J_A is removed during demagnetization levels 2 through 5; NRM component J_B is removed during demagnetization levels 7 through 9. (**b**) Vector component diagram resulting from progressive demagnetization of NRM composed of components J_A and J_B with demagnetization spectra shown in part (**a**). (**c**) Demagnetization spectra of the two NRM components with small interval of overlap. NRM component J_A is removed during demagnetization levels 2 through 6; NRM component J_B is removed during demagnetization levels 5 through 9. (**d**) Vector component diagram resulting from progressive demagnetization of NRM composed of components J_A and J_B with demagnetization spectra shown in part (**c**). (**e**) Demagnetization spectra of the two NRM components with large interval of overlap. NRM component J_A is removed during demagnetization levels 2 through 9; NRM component J_B is removed during demagnetization levels 3 through 9. (**f**) Vector component diagram resulting from progressive demagnetization of NRM composed of components J_A and J_B with demagnetization spectra shown in part (**e**). Modified from Dunlop (1979).

More than two components?

The majority of convincing paleomagnetic results have been obtained from rocks with no more than two components of NRM, usually a low-stability secondary NRM removed to allow isolation of a high-stability ChRM (often argued to be a primary NRM). However, a growing number of more complex NRMs with three or more components are being reported. As demagnetization procedures and analysis become more sophisticated and paleomagnetists venture into rocks with complex histories, reports of complex multicomponent NRMs will no doubt increase. It therefore seems important to show at least one example of a three-component NRM in which the components are probably interpretable.

In Figure 5.9, results of progressive demagnetization of Precambrian red argillite from the Belt Supergroup are illustrated. In this study, some specimens were demagnetized by using a combination of AF demagnetization followed by thermal demagnetization (proving once again that life gets complicated when dealing with Precambrian rocks). During AF demagnetization to 50 Oe (5 mT) peak field, a component of NRM is removed with direction $I \approx 50°$, $D \approx 15°$, subparallel to the geomagnetic field at the sampling locality. This low-stability component is probably a VRM.
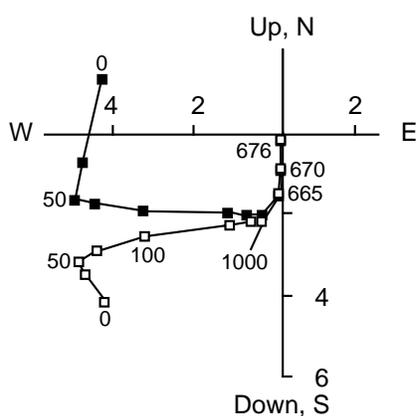
Figure 5.9 Vector component diagram on a three-component NRM. The sample is a red argillite from the Precambrian Spokane Formation of Montana; numbers on axes indicate NRM intensities in A/m; solid data points indicate projection onto the horizontal plane; open data points indicate projection onto the east-west oriented vertical plane; numbers 0 through 1000 indicate peak field (in Oe) used in alternating-field demagnetization; numbers 665 through 676 indicate temperatures (in degrees Celsius) used in subsequent thermal demagnetization. Modified from Vitorello and Van der Voo (*Can. J. Earth Sci.*, v. 14, 67–73, 1977).

During AF demagnetization between 50 Oe (5 mT) and 1000 Oe (100 mT), a component of intermediate stability is removed. The direction of this component is $I \approx 10°$, $D \approx 275°$. Thermal demagnetization of other samples revealed a similar intermediate-stability component with blocking temperatures in the 300° to 500°C interval. In addition, a high-stability ChRM found in many samples is isolated by thermal demagnetization in the 665° to 680°C interval. The ChRM is interpreted as a primary CRM acquired during (or soon after) deposition of these 1300 Ma argillites.

Using geological evidence for an Eocambrian metamorphic event in this region and favorable comparison of the direction of the intermediate-stability component with that predicted for Eocambrian age, this component was interpreted as the result of Eocambrian metamorphism. Although the paleomagnetists who made this observation were certainly diligent in their procedures, this example highlights the difficulty of securely interpreting multicomponent NRMs. The "degree of difficulty" in interpretation of paleomagnetic results increases as the power of the number of NRM components. Most examples discussed in this book are two-component NRMs, and we only occasionally venture into the realm of more complex multicomponent NRMs. However, it seems clear that much future paleomagnetic research will involve deciphering multicomponent NRMs that are encountered in old rocks with complex histories.

Principal component analysis

The examples of progressive demagnetization data in Figures 5.7 and 5.9 show that there is often significant scatter in otherwise linear trajectories of vector component diagrams. This is especially true for weakly

magnetized rocks and rocks for which ChRM is a small percentage of total NRM. A rigorous, quantitative technique is obviously needed to determine the direction of the best-fit line through a set of scattered observations. *Principal component analysis* (abbreviated p.c.a.) is the system that is in common use.

Consider the progressive thermal demagnetization data shown in Figure 5.10 (high temperature portion of thermal demagnetization of a Late Triassic red sediment). In the 600°C to 675°C interval, there is an obvious trend of data points toward the origin. Low-stability secondary components of NRM have been removed, and the only component remaining is the ChRM. But there is also considerable scatter. One might choose a single demagnetization level to best represent the ChRM (this was the method used until recently). However, it is preferable to use all the information from the five demagnetization temperatures by mathematically determining the best-fit line through the trajectory of those five data points. Kirschvink (see Suggested Readings) has shown how p.c.a. can provide the desired best-fit line. A qualitative understanding of p.c.a. is easily gained through the example of Figure 5.10. From a set of observations, p.c.a. determines the best-fitting line through a sequence of data points. In addition, a *maximum angular deviation* (MAD) is calculated to provide a quantitative measure of the precision with which the best-fit line is determined.

When fitting a line to data using p.c.a., there are three options regarding treatment of the origin of the vector component diagram: (1) force the line to pass through the origin ("anchored" line fit); (2) use the origin as a separate data point ("origin" line fit); or (3) do not use the origin at all ("free" line fit). For determination of ChRM, either anchored or origin line fits are commonly used because the ChRM is determined from a trend of data points toward the origin. In Figure 5.10, the anchored line fit to the data is shown. This is the best-fit line through the data determined by p.c.a. using the constraint that the line pass through the origin. The resulting line has direction $I = 6.4°$, $D = 162.8°$; and the MAD is 5.5°. If the data of Figure 5.10 are fit using an origin line fit, the resulting line has direction $I = 7.3°$, $D = 164.7°$, and the MAD is 8.0°.
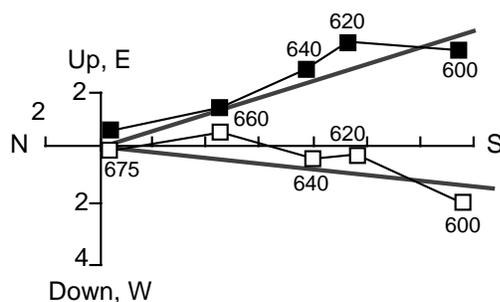
Figure 5.10 Example of best-fit line to progressive demagnetization data using principal component analysis. The sample is from the Late Triassic Chinle Formation of New Mexico; numbers on axes indicate NRM intensities in A/m; solid data points indicate projection onto the horizontal plane; open data points indicate projection onto the north-south oriented vertical plane; numbers adjacent to data points indicate temperatures of thermal demagnetization in degrees Celsius; the stippled lines show the best-fit direction ($I = 6.4°$, $D = 162.8°$) calculated by using the anchored option of principal component analysis applied to the data.

Note that maximum weight is put on the data points farthest from the origin because those points have maximum information content in determining the trend of the line. In an experimental context, the data points farthest from the origin are probably the best determined because the signal to noise ratio is greatest. Although no strict convention exists, line fits from p.c.a. that yield MAD ≥ 15° are often considered ill defined and of questionable significance.

Directions of secondary NRM also can be determined by using p.c.a. The low-stability component in Figure 5.7c or the intermediate-stability component of Figure 5.9 could be determined with this technique. For secondary NRM, the free line fit would be used because the trajectory on the vector component diagram does not include the origin.

For rocks with weak NRM or noisy trajectories during progressive demagnetization, p.c.a. can provide more robust determination of ChRM than using results from a single demagnetization level. If progressive

demagnetization studies of representative samples demonstrate straightforward isolation of the ChRM, re-maining samples would be treated at only one or two demagnetization levels to isolate the ChRM. This procedure is referred to as *blanket demagnetization.* However, if progressive demagnetization studies indicate weak or noisy ChRM, the remaining samples would be demagnetized at multiple demagnetization levels within the range that appears to isolate ChRM. Principal component analysis would be applied to the resulting data from all samples.

Advanced techniques

Some special techniques have been developed to deal with rocks for which ChRM cannot be isolated directly. Rocks with multiple components of NRM with severely overlapping spectra of blocking temperature or coercivity often yield arcs or *remagnetization circles* during progressive demagnetization. In special circumstances, these remagnetization circles may intersect at the direction of one of the NRM components. Several techniques for analysis of remagnetization circles have been developed and can sometimes pro-vide important information from rocks when more straightforward analysis fails. However, these techniques are complicated, generally require special geologic situations, and often yield unsatisfying results (complex magnetizations spawn complex interpretations). Some of these advanced techniques are referenced in the Suggested Readings.

FIELD TESTS OF PALEOMAGNETIC STABILITY

Laboratory demagnetization experiments reveal components of NRM and (usually) allow definition of a ChRM. Blocking temperature and/or coercivity spectra can suggest that ferromagnetic grains carrying a ChRM are capable of retaining a primary NRM. However, laboratory tests cannot prove that the ChRM is primary. *Field tests of paleomagnetic stability* can provide crucial information about the timing of ChRM acquisition. In studies of old rocks in orogenic zones, field test(s) of paleomagnetic stability can be the critical observation.

Common field tests of paleomagnetic stability are introduced here, and examples are presented. Through these examples, the logic and power of field tests can be appreciated. It is worth noting that quantitative evaluation of field tests requires statistical techniques for analyses of directional data that are developed in the next chapter.

The fold test

The *fold test* (or *bedding-tilt test*) and the *conglomerate test* are represented in Figure 5.11. In the fold test, relative timing of acquisition of a component of NRM (usually ChRM) and folding can be evaluated. If a ChRM was acquired prior to folding, directions of ChRM from sites on opposing limbs of a fold are dispersed when plotted in geographic coordinates (in situ) but converge when the structural correction is made ("re-storing" the beds to horizontal). The ChRM directions are said to "pass the fold test" if clustering increases through application of the structural correction or "fail the fold test" if the ChRM directions become more scattered. The fold test can be applied either to a single fold (Figure 5.11) or to several sites from widely separated localities at which different bedding tilts are observed.

An example of a set of ChRM directions which passes the fold test is shown in Figure 5.12. These directions are mean ChRM directions observed at five localities of the Nikolai Greenstone, part of the Wrangellia Terrane of Alaska. The ChRM directions in Figure 5.12a are uncorrected for bedding tilt (geo-graphic coordinates), while those in Figure 5.12b are after structural correction. This is a realistic example in the sense that bedding tilts are moderate. Improvement in clustering of ChRM directions upon application of structural correction is evident, if not dramatic, and passage of the fold test indicates that ChRM of the Nikolai Greenstone was acquired prior to folding. The ChRM directions also pass a reversals test (dis-cussed below), which helps to confirm that the ChRM of the Nikolai Greenstone is a primary TRM acquired
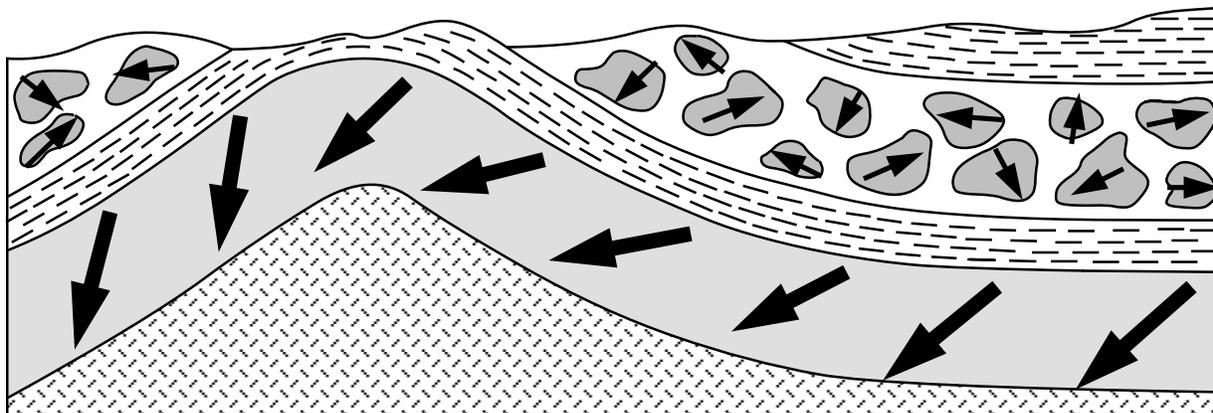
Figure 5.11 Schematic illustration of the fold and conglomerate tests of paleomagnetic stability. Bold arrows are directions of ChRM in limbs of the fold and in cobbles of the conglomerate; random distribution of ChRM directions from cobble to cobble within the conglomerate indicates that ChRM was acquired prior to formation of the conglomerate; improved grouping of ChRM upon restoring the limbs of the fold to horizontal indicates ChRM formation prior to folding. Redrawn from Cox and Doell (1960).
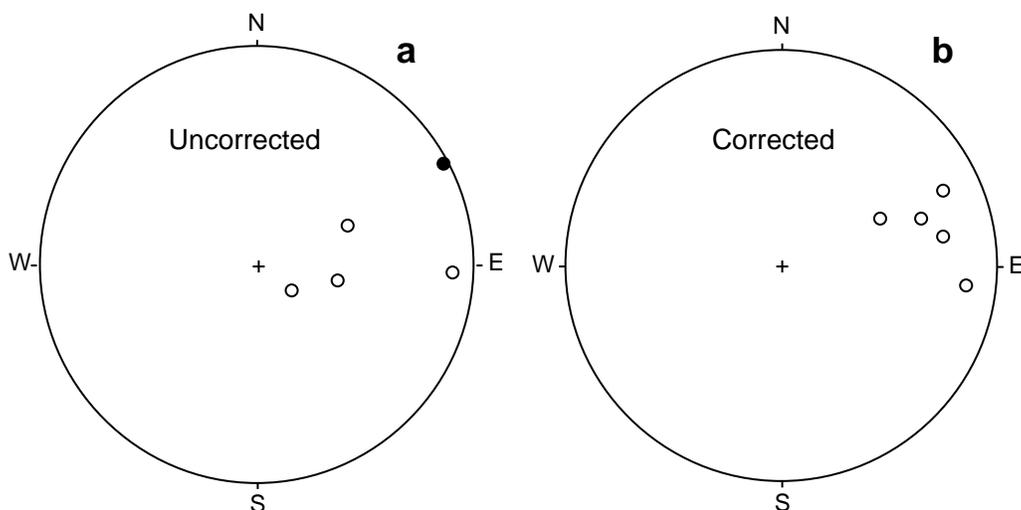
Figure 5.12 Example of ChRM directions that pass the fold test. Equal-area projections show mean ChRM directions from multiple sites at each of five collecting localities in the Nikolai Greenstone, Alaska; solid circles indicate directions in the lower hemisphere of the projection; open circles indicate directions in the upper hemisphere. (**a**) ChRM directions *in situ* (prior to structural correction). (**b**) ChRM directions after structural correction to restore beds to horizontal. Data from Hillhouse (*Can. J. Earth Sci.*, v. 14, 2578–2592, 1977).

during original cooling in the Middle–Late Triassic. This example also illustrates the necessity for a statistical test to allow quantitative evaluation of the fold test. (For example, at what level of certainty can we assert that the clustering of ChRM directions is improved by applying the structural corrections?)

Synfolding magnetization

Because an increasing number of cases of *synfolding magnetization* are being reported, the principles of synfolding magnetization are introduced, and an example is provided. In Figure 5.13a, observations expected for a prefolding magnetization are shown for a simple syncline. In Figure 5.13b, the observations
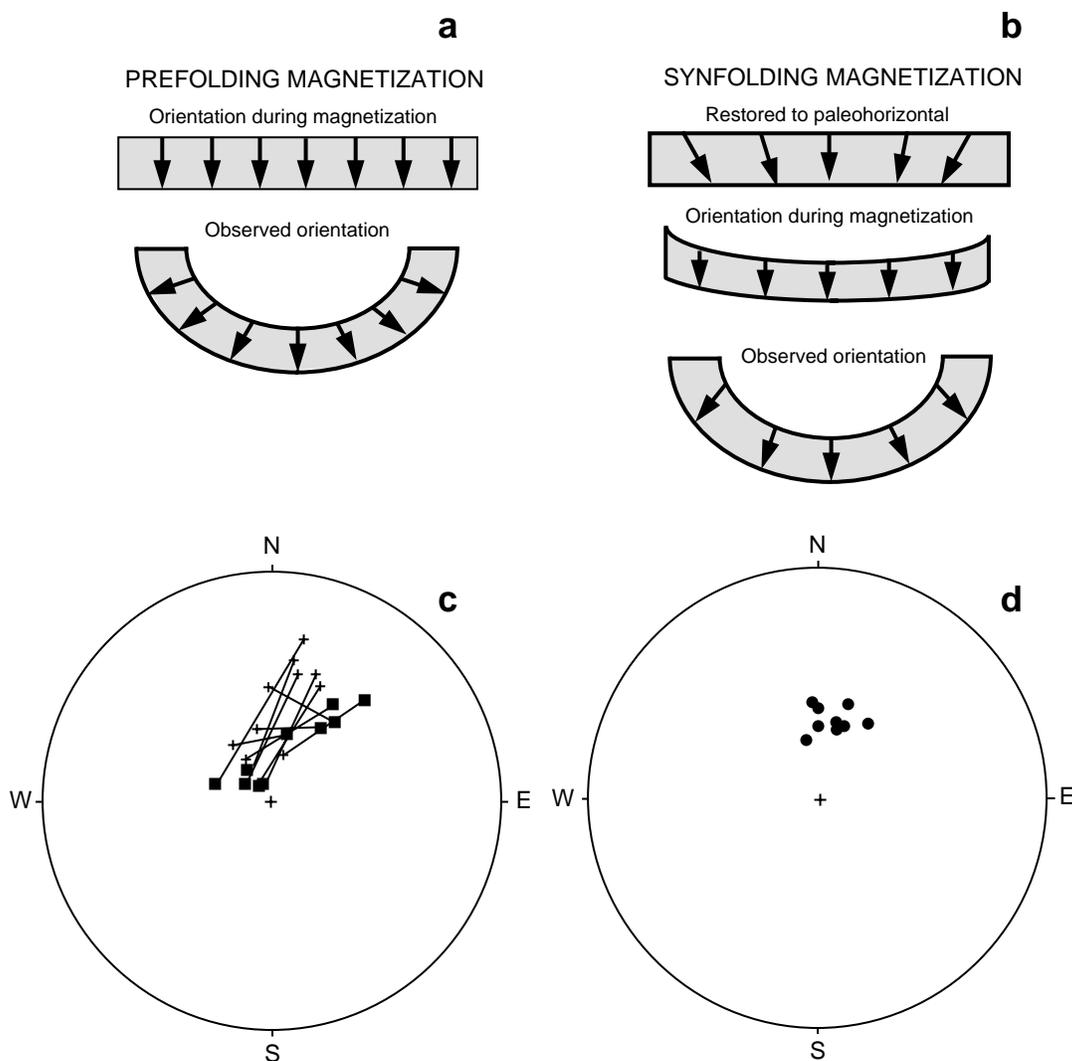
Figure 5.13 Synfolding magnetization. (**a**) Directions of ChRM are shown by arrows for pre-folding magnetization. ChRM directions are dispersed in the observed *in situ* orientation; restoring bedding to horizontal results in maximum grouping of the ChRM directions. (**b**) Directions of ChRM for synfolding magnetization. ChRM directions are dispersed in both the *in situ* orientation and when bedding is restored to horizontal; maximum grouping of the ChRM directions occurs when bedding is partially restored to horizontal. (**c**) Equal-area projection of directions of ChRM in Cretaceous Midnight Peak Formation of north-central Washington. Crosses are *in situ* site-mean ChRM directions for ten sites spread across opposing limbs of a fold; squares are site-mean ChRM directions resulting from restoring bedding at each site to horizontal; all directions are in the lower hemisphere of the projection. (**d**) Site-mean ChRM directions in Midnight Peak Formation after 50% unfolding. Data from Bazard et al. (*Can. J. Earth Sci.*, v. 27, 330–343, 1990).

expected for synfolding magnetization are represented. Observed directions of magnetization are shown in the bottom diagram of Figure 5.13b while the configuration of directions after complete unfolding is shown in the top diagram. Complete unfolding "overcorrects" the magnetization directions. The best grouping of the magnetization directions occurs when the structure is only partially unfolded, as in the middle diagram of Figure 5.13b. The inference drawn from such observations is that the magnetization was formed <u>during</u> formation of the syncline (synfolding magnetization).

In Figures 5.13c and 5.13d, an example of synfolding magnetization is shown. Mean directions of ChRM were determined for ten sites collected from localities spread across opposing limbs of a fold. In situ ChRM directions (geographic coordinates) are shown by crosses in Figure 5.13c, while ChRM directions after 100% unfolding are shown by squares. Inspection of Figure 5.13c reveals that ChRM directions from opposing limbs of the fold pass one another as the structural corrections are applied. Maximum clustering of ChRM directions occurs at 50% unfolding (Figure 5.13d). The conclusion is that the ChRM was most likely formed during folding. Again, quantitative assessment of the percentage of unfolding producing maximum clustering of ChRM directions requires use of a statistical method.

Conglomerate test

The *conglomerate test* is illustrated in Figure 5.11. If ChRM in clasts from a conglomerate has been stable since before deposition of the conglomerate, ChRM directions from numerous cobbles or boulders should be randomly distributed (= passage of conglomerate test). A nonrandom distribution indicates that ChRM was formed after deposition of the conglomerate (= failure of conglomerate test). Passage of the conglomerate test indicates that the ChRM of the source rock has been stable at least since formation of the conglomerate. A positive conglomerate test from an intraformational conglomerate provides very strong evidence that the ChRM is a primary NRM.

The Glance Conglomerate of southern Arizona is an interbedded sequence of silicic volcanic and sedimentary rocks including conglomerate. Randomly distributed ChRM directions observed in volcanic cobbles of a conglomerate are shown in Figure 5.14. Because this conglomerate is <u>within</u> the sequence of volcanic flows of the Glance Conglomerate, passage of the conglomerate test indicates that ChRM directions in the volcanic rocks are primary.
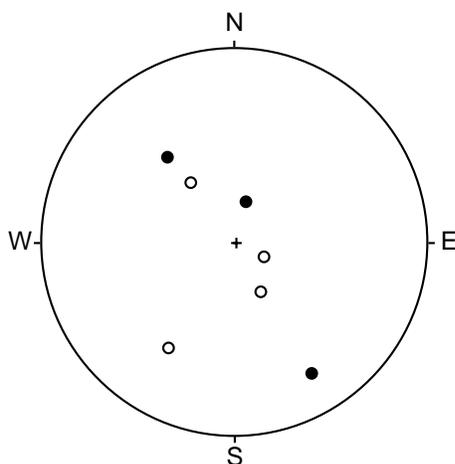
Figure 5.14 Example of ChRM directions that pass the conglomerate test. The equal-area projection shows the ChRM directions in seven volcanic cobbles in a conglomerate within a sequence of volcanic flows of the Late Jurassic Glance Conglomerate; open circles are directions in the upper hemisphere; solid circles are directions in the lower hemisphere; the ChRM directions are randomly distributed, indicating ChRM formation prior to incorporation of the cobbles in the conglomerate. Redrawn from Kluth et al. (*J. Geophys. Res.*, v. 87, 7079–7086, 1982).

If processes of weathering associated with conglomerate formation have resulted in alteration of the ferromagnetic minerals, the conglomerate test can be negative even when the source rock contains a stable ChRM. Passage of a conglomerate test thus provides strong evidence for stability, whereas failure of the test is certainly a warning, but not necessarily a clear indication that the ChRM of the source rock is secondary.

Reversals test

As explained in Chapter 1, the time-averaged geocentric axial dipolar nature of the geomagnetic field holds during both normal- and reversed-polarity intervals. At all locations, the <u>time-averaged</u> geomagnetic field directions during a normal-polarity interval and during a reversed-polarity interval differ by 180°. This property of the geomagnetic field is the basis for the *reversals test* of paleomagnetic stability shown schematically in Figure 5.15.

Reversals Test

Reversed   Normal

⟶ Primary

⟶ Secondary

⟶ Resultant
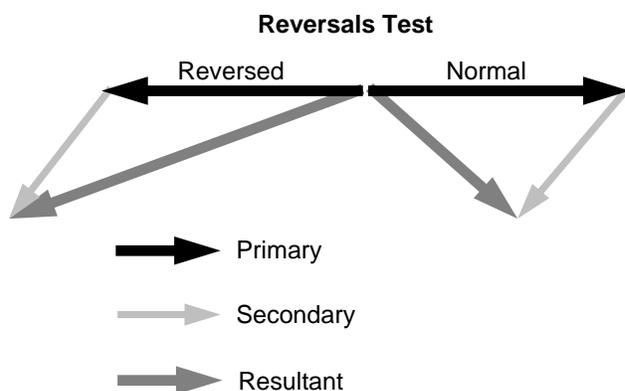
Figure 5.15 Schematic illustration of the reversals test of paleomagnetic stability. Solid arrows indicate the expected antiparallel configuration of the average direction of primary NRM vectors resulting from magnetization during normal- and reversed-polarity intervals of the geomagnetic field; an unremoved secondary NRM component is shown by the lightly stippled arrows; the resultant NRM directions are shown by the heavily stippled arrows. Redrawn from McElhinny (*Palaeomagnetism and Plate Tectonics*, Cambridge, London, 356 pp., 1973).

If a suite of paleomagnetic sites affords adequate averaging of secular variation during both normal- and reversed-polarity intervals, the average direction of primary NRM for the normal-polarity sites is expected to be antiparallel to the average direction of primary NRM for the reversed-polarity sites. However, acquisition of later secondary NRM components will cause resultant NRM vectors to deviate by less than 180°. ChRM directions are said to "pass the reversals test" if the mean direction computed from the normal-polarity sites is antiparallel to the mean direction for the reversed-polarity sites. Passage of the reversals test indicates that ChRM directions are free of secondary NRM components and that the time sampling afforded by the set of paleomagnetic data has adequately averaged geomagnetic secular variation. Furthermore, if the sets of normal- and reversed-polarity sites conform to stratigraphic layering, the ChRM is probably a primary NRM.

If a paleomagnetic data set "fails the reversals test," the average directions for the normal and reversed polarity sites differ by an angle that is significantly less than 180°. Failure of the reversals test can indicate either (1) presence of an unremoved secondary NRM component or (2) inadequate sampling of geomagnetic secular variation during either (or both) of the polarity intervals. Because polarity reversals are characteristic of most geologic time intervals, paleomagnetic data sets often contain normal- and reversed-polarity ChRM. The reversals test of paleomagnetic stability is often applicable and, unlike the conglomerate or fold test, does not require special geologic settings.

An example of the reversals test is shown in Figure 5.16, which displays mean ChRM directions from Paleocene continental sediments of northwestern New Mexico. The mean ChRM direction from 42 normal-polarity sites is antiparallel to the mean ChRM direction of 62 reversed-polarity sites. The ChRM directions thus pass the reversals test for paleomagnetic stability. Quantitative evaluation of the reversals test involves computation of the mean directions (and confidence intervals about those mean directions) for both normal- and reversed-polarity groups and comparison of one mean direction with the antipode of the other mean direction. Statistical methods for such comparisons are developed in the next chapter.

Baked contact and consistency tests

Baked zones of country rock adjacent to igneous rocks allow application of the *baked contact test* of paleomagnetic stability. The baked country rock and igneous rock acquire a TRM that should agree in direction. Mineralogies of the igneous rock and adjacent baked country rock can be very different, with different tendencies for acquisition of secondary NRM and different demagnetization procedures required for isolation of ChRM. Agreement in ChRM direction between an igneous rock and adjacent baked country rock thus provides confidence that the ChRM direction is a stable direction that may be a primary NRM. For country rock that is much older than the igneous rock, ChRM directions in unbaked country rock are expected to be significantly different from the ChRM direction of the igneous rock. Thus similar ChRM directions for igneous rock and baked country rock but a distinct ChRM direction from unbaked country rock constitute pas-
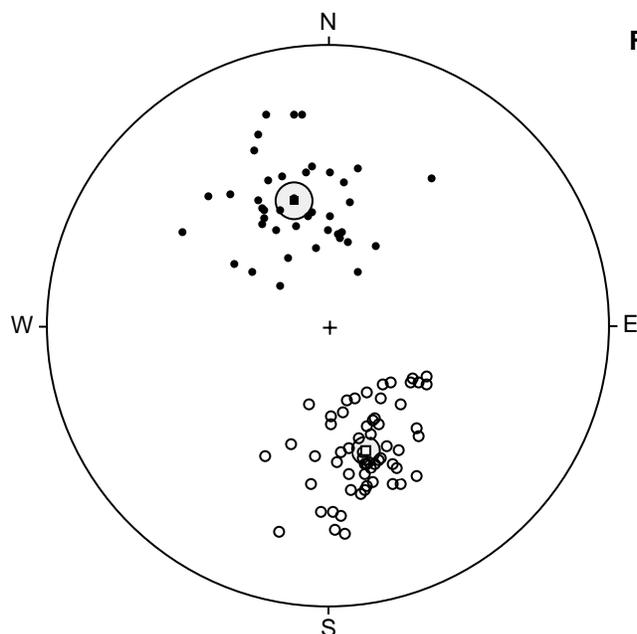
Figure 5.16 Example of ChRM directions that pass the reversals test of paleomagnetic stability. Equal-area projection of site-mean ChRM directions from 104 sites in the Paleocene Nacimiento Formation of northwestern New Mexico; solid circles are directions in the lower hemisphere of the projection; open circles are directions in the upper hemisphere; the mean of the 42 normal-polarity sites is shown by the solid square with surrounding stippled circle of 95% confidence; the mean of the 62 reversed-polarity sites is shown by the open square with surrounding stippled circle of 95% confidence; the antipode of the mean of the reversed-polarity sites is within 2° of the mean of the normal-polarity sites (within the confidence region). Redrawn from Butler and Taylor (*Geology*, v. 6, 495–498, 1978).

sage of the baked contact test. Uniform ChRM directions for igneous rock, baked zone, <u>and</u> unbaked country rock could indicate widespread remagnetization of all lithologies.

The *consistency test* for paleomagnetic stability involves observation of the same ChRM direction (remote from the present geomagnetic field direction) for different rock types of similar age. If mineralogies of the ferromagnetic minerals are highly variable and demagnetization procedures required for isolation of ChRM are different, but ChRM direction depends on geologic age, these observations are "consistent with the interpretation that the ChRM is a primary NRM." Obviously, this consistency test must be accompanied by other indicators of stability of paleomagnetism because a consistent direction of ChRM could also indicate wholesale remagnetization of the region.

SUGGESTED READINGS

INSTRUMENTATION AND LABORATORY TECHNIQUES:
D. W. Collinson, *Methods in Rock Magnetism and Palaeomagnetism*, Chapman and Hall, London, 503 pp., 1983.
> *Theory, instrumentation, and techniques of partial demagnetization are covered in considerable detail.*

CONVERGING REMAGNETIZATION CIRCLES:
H. C. Halls, A least-squares method to find a remanence direction from converging remagnetization circles, *Geophys. J. Roy. Astron. Soc.*, v. 45, 297–304, 1976.
H. C. Halls, The use of converging remagnetization circles in palaeomagnetism, *Phys. Earth Planet. Int.*, v. 16, 1–11, 1978.
> *Present theory and applications of remagnetization circle analysis.*

VECTOR COMPONENT DIAGRAMS AND PRINCIPAL COMPONENT ANALYSIS:
D. J. Dunlop, On the use of Zijderveld vector diagrams in multicomponent paleomagnetic samples, *Phys. Earth Planet. Sci. Lett.*, v. 20, 12–24, 1979.
> *Powers and limitations of vector component diagrams are discussed with many examples given.*
J. D. A. Zijderveld, A.C. demagnetization of rocks: Analysis of results, In: *Methods in Palaeomagnetism*, ed D. W. Collinson, K. M. Creer, and S. K. Runcorn, Elsevier, Amsterdam, pp. 254–286, 1967.
> *This paper introduces the technique of vector component diagrams.*
K. A. Hoffman and R. Day, Separation of multicomponent NRM: A general method, *Earth Planet. Sci. Lett.*, v. 40, 433–438, 1978.
> *An advanced look at separation of components.*

J. L. Kirschvink, The least-squares line and plane and the analysis of palaeomagnetic data, *Geophys. J. Roy. Astron. Soc.*, v. 62, 699–718, 1980.
>   *Paleomagnetic applications of principal component analysis.*

J. T. Kent, J. C. Briden, and K. V. Mardia, Linear and planar structure in ordered multivariate data as applied to progressive demagnetization of palaeomagnetic remanence, *Geophys. J. Roy. Astron. Soc.*, v. 75, 593–621, 1983.
>   *An advanced treatment of statistical analysis of progressive demagnetization data.*

FIELD TESTS OF PALEOMAGNETIC STABILITY:

E. Irving, *Paleomagnetism and Its Application to Geological and Geophysical Problems*, Wiley & Sons, New York, 399 pp., 1964.
>   *Chapter 4 presents a very useful discussion of the development and application of field tests.*

J. W. Graham, The stability and significance of magnetism in sedimentary rocks, *J. Geophys. Res.*, v. 54, 131–167, 1949.
>   *A classic paper which introduces several field tests.*

A. Cox and R. R. Doell, Review of Paleomagnetism, *Geol. Soc. Amer. Bull.*, v. 71, 645–768, 1960.
>   *Several illustrations of field tests are presented.*

PROBLEMS

5.1   A diagram (Figure 5.2) plotting SD grain volume, v, versus microscopic coercive force, h_c, was used to explain the theory of thermal demagnetization. Part of that diagram is shown in Figure 5.17. Using this v–h_c diagram, develop a qualitative explanation for the observation that AF demagnetization generally fails to remove VRM from rocks with hematite as the dominant ferromagnetic mineral.
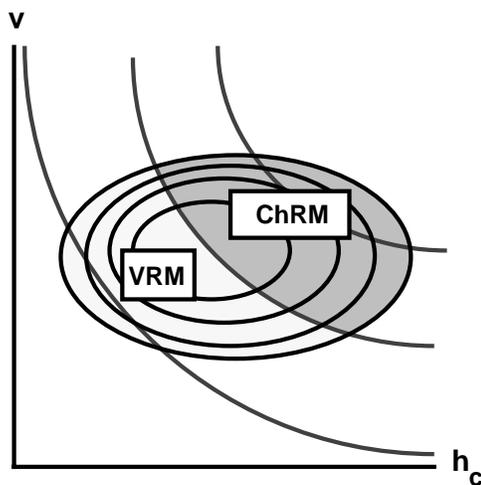
Figure 5.17 Grain volume (v) versus microscopic coercive force (h_C) for a hypothetical population of SD grains. Symbols and contours as in Figure 5.2.

5.2   Vector component diagrams illustrating progressive demagnetization data for two paleomagnetic samples are shown in Figure 5.18. These samples are from volcanic rocks containing magnetite as the dominant ferromagnetic mineral.
>   **a**.   Using a protractor to measure angles of line segments in Figure 5.18a, estimate the direction of the ChRM revealed by this progressive demagnetization experiment.
>   **b**.   Applying the same procedure to Figure 5.18b, estimate the direction of the <u>secondary</u> component of NRM that is removed between AF demagnetization levels 2.5 mT and 10 mT.

5.3   Paleomagnetic samples were collected at two locations within a Permian red sedimentary unit. This unit is gently folded and overlain by flat-lying Middle Triassic limestones. There is no evidence suggesting plunging folds. The present geomagnetic field direction in the region of collection is $I = 60°$, $D = 16°$. At site 1, six samples were collected, and the NRM directions are listed below. Bedding at site 1 has the following attitude: dip = 15°, dip azimuth = 130° (strike = 220°). After thermal demagnetization, the ChRM directions of the samples from site 1 cluster about a direction $I = -4°$, $D = 165°$. At site 2, six samples were also collected, and the measured NRM directions are
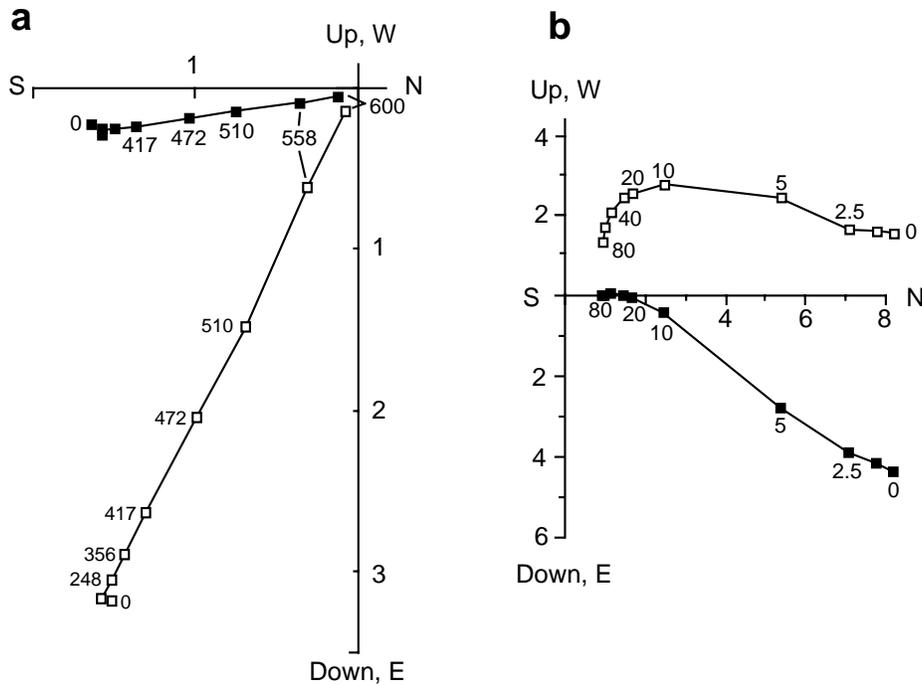
Figure 5.18 Vector component diagrams. (**a**) Progressive thermal demagnetization results for one sample; the numbers adjacent to data points are temperatures in degrees Celsius; open data points are vector end points projected onto a north-south oriented vertical plane; solid data points are vector end points projected onto the horizontal plane; numbers on axes are in A/m. (**b**) Progressive AF demagnetization results for another sample. Conventions and labels as for part (**a**), except that numbers adjacent to the data points indicate H_{AF} (in mT); the NRM of this sample contains a large secondary lightning-induced IRM.

listed below. Bedding at site 2 has the following attitude: dip = 20°, dip azimuth = 290° (strike = 20°). After thermal demagnetization, the ChRM directions of the samples from site 2 cluster about a direction $I = -28°$, $D = 174°$. From these data, what can you conclude about (1) the presence of secondary components of NRM, (2) the likely origin of any secondary components of NRM, (3) the age of the ChRM? You will want to illustrate your answer by plotting directions on an equal-area projection.

Site 1 NRM Directions:		Site 2 NRM Directions:	
I (°)	D (°)	I (°)	D (°)
−2	164	−27	174
37	151	62	158
10	162	−20	175
31	154	76	94
69	46	−11	175